Atmospheric He/O2 plasma jet fine etching with a scanning probe microscope

メタデータ	
	言語: eng
	出版者:
	公開日: 2020-09-14
	キーワード (Ja):
	キーワード (En):
	作成者: Nakazawa, Kenta, Yamamoto, Sho, Nakagawa, Ei, Ogino, Akihisa, Shimomura, Masaru, Iwata, Futoshi
	メールアドレス:
	所属:
URL	http://hdl.handle.net/10297/00027686

Atmospheric He/O₂ plasma jet fine etching with a scanning probe microscope

Kenta Nakazawa,[1] (ID) Sho Yamamoto,[1] Ei Nakagawa,[1] Akihisa Ogino,[1] Masaru Shimomura,[1] (ID)
and Futoshi Iwata[1,2,3,a] (ID)

AFFILIATIONS

[1] Graduate School of Integrated Science and Technology, Shizuoka University, Johoku 3-5-1, Naka-ku, Hamamatsu 432-8561, Japan
[2] Graduate School of Medical Photonics, Shizuoka University, Johoku 3-5-1, Naka-ku, Hamamatsu 432-8011, Japan
[3] Research Institute of Electronics, Shizuoka University, Johoku 3-5-1, Naka-ku, Hamamatsu 432-8011, Japan

[a] Author to whom correspondence should be addressed: iwata.futoshi@shizuoka.ac.jp

ABSTRACT

In this study, we investigate a maskless fine etching technology using a He/O₂ atmospheric pressure plasma jet (APPJ) assisted by a scanning probe microscope (SPM). The APPJ is localized in the submicrometer range by a nanopipette, which is also used as the probe of the SPM. We improve the rate of submicrometer-scale etching by adding O₂ gas to the He source gas. The depth and full width at half maximum of a typical etched dot on a polymethylmethacrylate film were 475 nm and 235 nm, respectively. The etching rate was found to be six times faster with the added gas than without it. We also demonstrate line patterning; the width of the line was found to be 281 nm.

I. INTRODUCTION

Plasma generated under atmospheric pressure has gained significant attention in various fields such as physics,[1,2] engineering,[3,4] medicine,[5,6] and biology.[7,8] Particularly in engineering, the atmospheric pressure plasma jet (APPJ) has a significant application potential in microfabrication and nanofabrication technologies. It has attractive advantages such as the generation of high-density plasma without a vacuum system and localization of the processing area. As the APPJ can be easily localized, it is useful for the maskless fabrication processes. In general, the APPJ is generated in a dielectric tube and irradiated as a plasma bullet from the tube end.[9] By reducing the diameter of the tube end down to the order of micrometers or nanometers, the APPJ can be localized to an equivalent size. In a previous study, a special microcantilever with a plasma nozzle in the pyramidal tip has also been used for the localization of the APPJ.[10]

The deposition[11–13] and etching processes[14–16] have been developed using the APPJ in previous studies. Ichiki et al. reported a maskless etching process for silicon using an inductively coupled APPJ. As the etching gas, SF₆ was excited by the APPJ to remove silicon. The etching rate and diameter of the etched dots were 200 μm/min–600 μm/min and 400 μm–600 μm, respectively. This etching rate is very high compared with those of conventional etching processes in vacuum.[17]

For nanometer-scale processing, the nozzle must be finely positioned with an aperture of nanometer-sized diameter with respect to the etching material surface.[18–20] We have previously developed an atmospheric plasma jet etcher assisted by a scanning probe microscope (SPM) with a nanopipette.[21] The SPM was used for fine-positioning the nanopipette employed as the APPJ nozzle. In a previous report, a photoresist polymer was removed by a He APPJ. However, it is difficult to remove other polymer materials, such as polymethylmethacrylate (PMMA), with the exception of photoresist polymers. For fine processing, the nanopipette should be in the vicinity of the surface of the substrate within the submicrometer range. Therefore, it is difficult to excite ambient air containing a reactive gas such as O₂ to remove polymers. To overcome the limitations of the processing materials that are used in the nanometer-scale APPJ, etching gases are added, which holds significant potential.

Furthermore, it is essential to investigate the emission spectrum of the plasma. In the case of APPJ, optical emission spectroscopy is often utilized to identify the reactive species in the plasma.[22–24]

In this study, we developed a fine processing method in the submicrometer range using the APPJ with He and additive gases assisted by a scanning probe microscope. The PMMA films, which are difficult to remove using the APPJ with pure He, are used as etching samples. As an etching gas, O$_2$ is added to He, which is used as plasma source gas. By adding O$_2$ gas, oxygen radicals are

generated and PMMA films are removed due to the decomposition of PMMA, which is mainly composed of carbon. Furthermore, the optical emission spectrum was measured at the tip of the nanopipette. In Sec. II, the principle of the fine processing system and the etcher that was developed are described. The effectiveness of the additive gas, the dependence of the additive gas ratio on the etching rate, and the line patterning are described in Sec. III. The experimental results are discussed in Sec. IV. We conclude this paper in Sec. V.
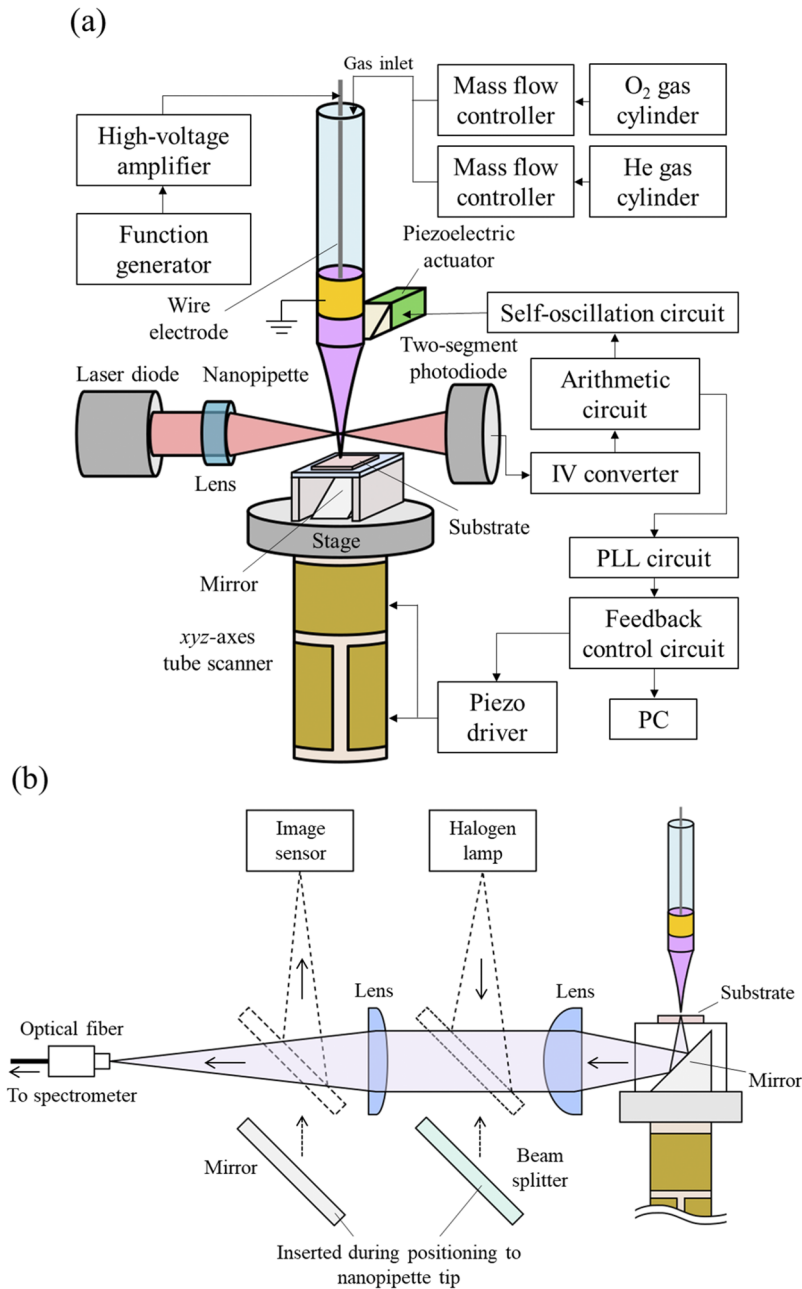
FIG. 1. Schematics of (a) etching system and (b) optical system for optical emission spectroscopy of the APPJ on the nanopipette.

II. ATMOSPHERIC PRESSURE PLASMA JET ETCHING SYSTEM

A schematic of the atmospheric plasma etching system is presented in Fig. 1. The system is composed of a nanopipette positioning unit based on the frequency-modulated SPM and the plasma generation unit. The nanopipette is a key element of the setup; it is used as the nozzle for localizing the plasma in the submicrometer scale and the probe in the SPM system that can measure the surface profile. The nanopipette was fabricated from a capillary glass tube (G-1, Narishige) using a laser pipette puller (P-2000, Sutter Instrument). In this study, PMMA was employed as the etching material. PMMA dissolved in 1,2-dichloroethane was coated on a glass substrate and baked on a hotplate at 120 °C for 50 min to remove the solution.

In the positioning unit, share force detection is employed. Share force is generated between the tip of the nanopipette and the material surface film on the substrate that is mounted on the xyz-axes piezoelectric tube stage (Z60H9.8×11C-EYXN, FUJI CERAMICS). The share force strongly increases when the tip of the nanopipette approaches the vicinity of the surface. Thus, the resonant frequency of the nanopipette decreases. The position at which the resonant frequency decreases down to the predetermined threshold is defined as the original position. The mechanical vibration at the resonant frequency is excited by a piezoelectric actuator (Z2T3×3S-LLYX, FUJI CERAMICS) controlled by a self-oscillation controller (OC4, Nanonis). The laser beam focused on the vibrating nanopipette edge was projected onto a two-segment photodiode (S4602, Hamamatsu Photonics). The shadow of the nanopipette vibrates in the laser spot, oscillating the subtracted signal of the two-segment photodiode. The amplitude of the nanopipette vibration was measured from the oscillation signal of the photodiode. A laser diode (LDV167S, TAKEX) and plano–convex lens with a focal length of 15 mm were utilized. The signal from the photodiode is input to the phase-locked loop circuit and proportional-integral (PI) controller (SC4, Nanonis) through a customized current-to-voltage (IV) converter and arithmetic circuit. The PMMA film and nanopipette are charged by APPJ irradiation. The surface charge influences the share force detection. In order to remove the surface charge, soft x-ray was irradiated to generate photoionization (L12645, Hamamatsu Photonics) before measuring the surface profile.

The plasma generation unit consists of a high-voltage supply and a gas supply. A tungsten wire electrode was introduced in the nanopipette channel. The grounded electrode was prepared on the circumference of the capillary glass. A high-voltage rectangular wave generated by a function generator (WF1974, NF) was applied to the wire electrode through a high-voltage amplifier (HV4321, NF). The He source gas for plasma generation and O_2 gas for reactive species generation were introduced in the nanopipette. These gases were supplied from gas cylinders. Their flow rates were individually controlled using mass flow controllers. Owing to the difficulty of controlling the flow rates of the gases using a nanopipette, a vent opening was fabricated before the inflow of the nanopipette.

The optical system used for optical emission spectroscopy is illustrated in Fig. 1(b). This system consists of two parts: an imaging part for alignment to the tip of the nanopipette and a spectroscopy part. Plano–convex lenses made of quartz were used as the objective and imaging lenses. The focal length and diameter of the object lens were 30 mm and 25 mm, respectively; those of the imaging lens were 80 mm and 20 mm, respectively. The emission light was guided by an optical fiber to the spectrometer (FLAME-S, Ocean Optics).

III. EXPERIMENTAL RESULTS

The effectiveness of introducing the additive O_2 gas is described. The etching profile of the dots fabricated by the irradiation of the APPJ with and without the additive O_2 gas is shown in Fig. 2. It was measured using the same nanopipette probe as the nozzle to localize the irradiation spot of the APPJ. The flow rates of the He and O_2 gases were 0.4 SLM and 5 SCCM, respectively. In all other experiments, the flow rate of He gas for plasma generation was 0.4 SLM. The peak-to-valley applied voltage for plasma generation was 4 kV_{PP} at a frequency of 7 kHz. The distance between the nanopipette tip and the surface of the substrate is 0.2 μm. As illustrated in Fig. 2, the plasma is irradiated for 2 s in five positions; the first, third, and fifth from the left-hand side of Fig. 2(a) are dots etched by the irradiation of the plasma of the He source gas with O_2 gas, and the second and fourth are dots irradiated by the plasma without the added O_2 gas. The areas irradiated by the plasma containing O_2 gas were locally etched. The typical depth and full width at half maximum (FWHM) of the etched dots were 475 nm and 235 nm, respectively. On the other hand, the PMMA film was removed only slightly from the area irradiated by the plasma without O_2 gas. The depths of the
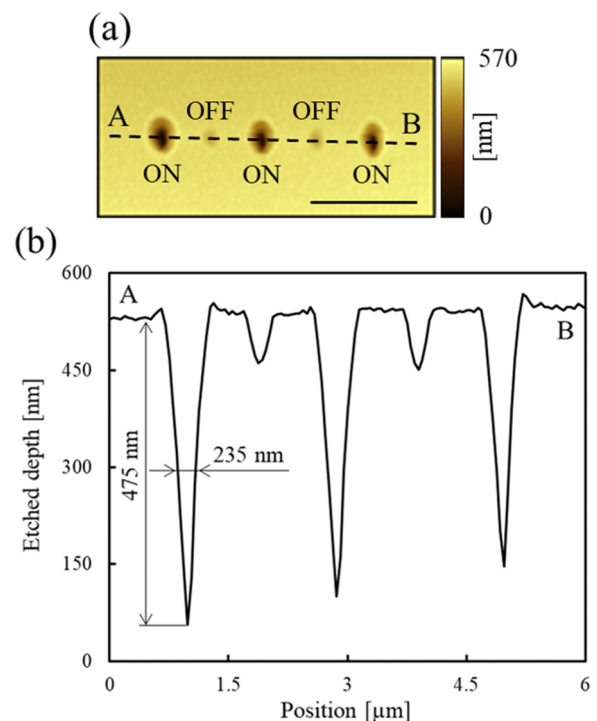

FIG. 2. (a) Topological image and (b) surface profile of the etched PMMA film measured using the SPM. Scale bar in the topological image is 2 μm.

dots etched without O_2 gas were significantly lower when compared with those etched with O_2 gas. By introducing O_2, the PMMA film was removed up to 6 times the depth in the area irradiated with plasma containing the additive O_2 gas. Therefore, it is established that the additive gas is effective for etching the PMMA film. The investigation of the etching conditions in the presence of the additive will be described.

The generation of radicals affecting PMMA removal was investigated using optical emission spectroscopy. As PMMA is mainly composed of carbon, it reacts with oxygen radicals and is removed as carbon oxide. The optical emission spectra of the APPJ at the nanopipette tip with flow rates of 0 SCCM and 1 SCCM for O_2 gas are presented in Figs. 3(a) and 3(b), respectively. In both cases, the applied voltage was 4 kV_{pp} at a frequency of 7 kHz. To obtain the spectra, the required integration time of the spectrometer was 0.5 s. The spectra from 330 nm to 430 nm, and 588 nm and 707 nm belong to N_2, and He gases, respectively. Note that the strong spectrum at 673 nm is irradiated from the laser diode for positioning the nanopipette. Here, we focus on the O atom with an emission wavelength of 777 nm.[25] The spectrum of the O atom was detected under both O_2 flow rate conditions. This suggests that the O atom is generated not only from the additive O_2 gas in the nanopipette but also from the O_2 in the air. The emission intensity of the O atom with a

flow rate of 1 SCCM is 1.5 times larger when compared with that of 0 SCCM.

Figure 4 shows the dependence of the plasma irradiation time on the depth of the etched dots. The flow rate of the O_2 gas was 5 SCCM. A voltage of 3 kV_{pp} was applied at 7 kHz. Figure 4(a) presents the topological image and surface profiles of the dots fabricated with different etching times. Based on the surface profiles, the depths of the etched dots as a function of the etching time are plotted in Fig. 4(b). The two dots were fabricated each under etching time conditions. The averaged etched depth was plotted in Fig. 4(b). The etching depth increases with increasing irradiation time. The etching rate can be obtained from this figure, which is essential for estimating the etching depth. Assuming that the etching depth is linearly proportional to the irradiation time, an etching rate of 268 nm/s is obtained.

The relationship between the amount of O_2 gas introduced and the depth of the etched dots for the etching time of 0.3 s is shown in Fig. 5. Voltages of 3.0, 3.5, and 4.0 kV_{pp} were applied. Four experiments were conducted under each condition, and the plots of the mean values are presented in Fig. 5. When the flow rate of O_2 gas was 1 SCCM, the etching depth increased for the following order of voltages of 4.0, 3.5, and 3.0 kV_{pp}. The depths of the etched dots at 3.0, 3.5, and 4.0 kV_{pp} were 17 nm, 59 nm, and 103 nm, respectively.
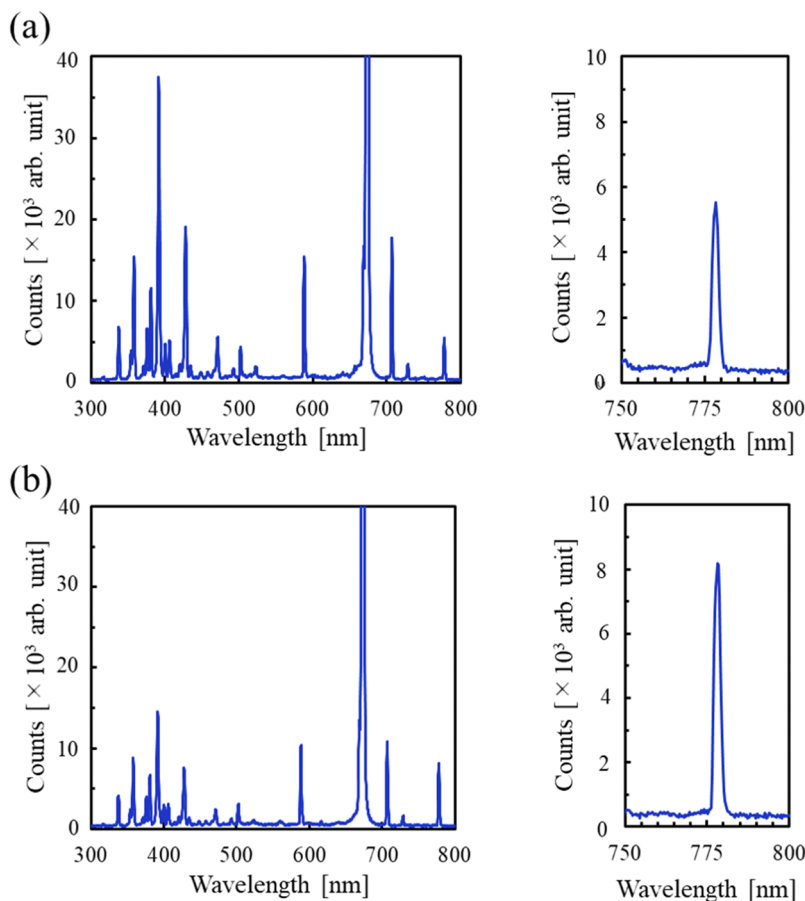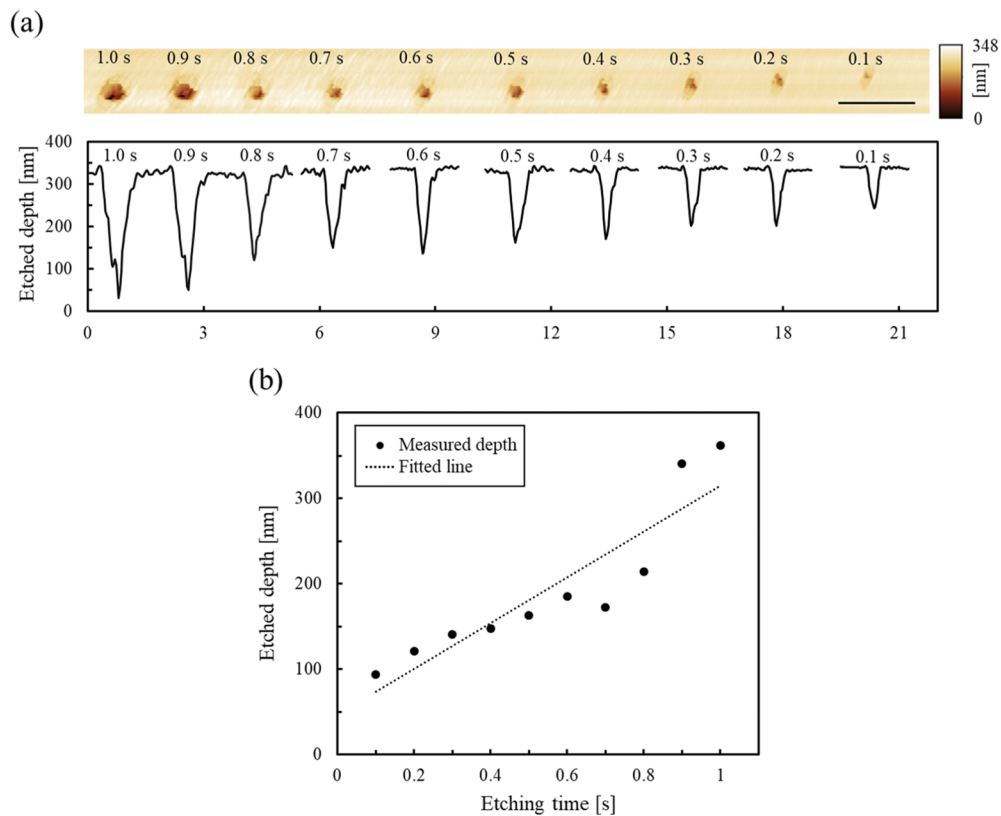

FIG. 3. Optical emission spectra at the O_2 flow rate of (a) 0 SCCM and (b) 1 SCCM.

FIG. 4. Dependence of depth of etched dots on etching time: (a) topological image measured using the SPM and (b) plot of depth of etched dots measured using the SPM for etching time of 0.1 s–1 s. Scale bar is 2 μm in the topological image.

Thus, the higher the input energy, the higher the etching rate. The depths of the etched dots did not increase linearly with the increasing flow rate of O_2 gas at the three levels of the applied voltage. At 3.0 and 3.5 kV$_{pp}$, the gradient decreased from 5 SCCM to 7 SCCM, and
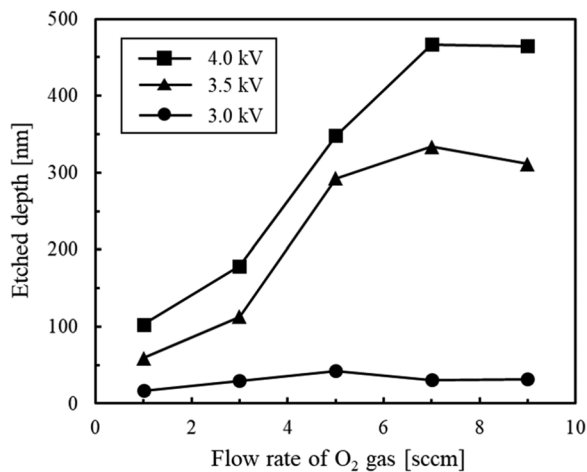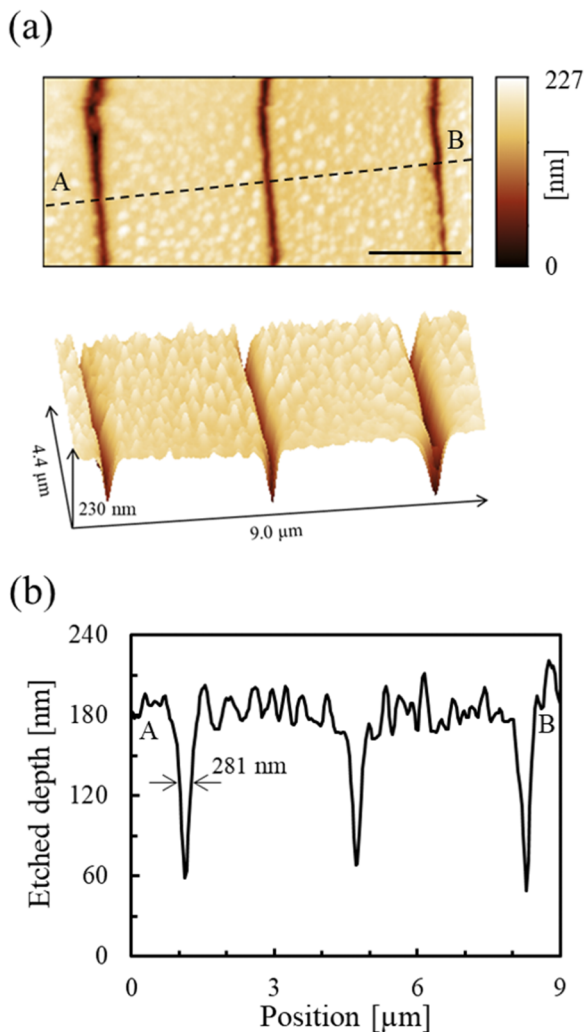

FIG. 5. Dependence of the O_2 flow rate on etched depth.

at 4.0 kV$_{pp}$, it decreased from 7 SCCM to 9 SCCM. Therefore, it is necessary to investigate the flow rate of O_2 gas at the applied voltage to maximize the etching rate. The dependence of the etching rate on the flow rate of O_2 is discussed in Sec. IV.

For the application of this etching system, complex 2D patterning is required. Dot patterning was performed to investigate the basic etching characteristics. Line patterning was also demonstrated. Figure 6 demonstrates line patterning on a PMMA film using the He/O_2 plasma. Three parallel lines were patterned. The flow rate of O_2 gas and applied voltage were 5 SCCM and 4 kV$_{pp}$ at 7 kHz, respectively. The stage was moved at a speed of 5 μm/s. As shown in Fig. 6(b), the FWHM of the line width is 281 nm, which is close to the diameter of the aperture of the nanopipette.

IV. DISCUSSION

In our experiment, it was confirmed that the etching rate improved as the flow rate of the added O_2 gas to the He plasma source gas was increased. However, as shown in Fig. 5, the etching rate did not increase when the flow rate of O_2 increased above 7 SCCM under an applied voltage of 3.5 kV$_{pp}$. This observation is attributed to two factors. The first is that the APPJ becomes unstable with the increase in the flow rate of O_2. To generate an APPJ, monoatomic gases such as He and Ar are often used because they are

FIG. 6. Line patterning: (a) topological image measured using the SPM and (b) cross-sectional surface profile of line patterning. Scale bar is 2 μm in the topological image.

plasma increases. The results of the measurement of the density of O atom, O_3, and O_2 in the He/O_2 APPJ using molecular beam mass spectroscopy were reported by Ellerweg et al.[27] The reported simulation and measurement results qualitatively explain our results. To optimize the etching rate, the combination of the conditions of the flow rate of O_2 and applied voltage is significant. To reduce the consumption of O_2, it should be introduced in the APPJ at the critical flow rate.

The line patterning and patterned groove width are described in Fig. 6. In a previous study, dot etching of a parylene-C film using an He/O_2 APPJ was reported.[20] Similar to our study, a nanopipette with an aperture of 10 μm in diameter was employed to localize the APPJ. The diameters and depths of the dots fabricated with an etching time of 2 min were 45 μm–56 μm and 1.8 μm–2.8 μm, respectively. Compared with this previous study, our system is more suitable for finer processing owing to the nanometer-scale precision positioning system and submicrometer-scale localized APPJ. Ellerweg et al. reported that the density of the reactive species in an APPJ is lower downstream of the jet than upstream.[27] Therefore, the position of the APPJ irradiated on the etching film may impact the etching resolution.

In our previous study,[21] the scanning speed of the line patterning on a photoresist polymer with the He APPJ (without additive O_2) was 0.5 μm/s. In this study, the scanning speed line patterning on the PMMA film was 5 μm/s with the He/O_2 APPJ. The etching rate of photoresist polymers is generally faster than that of PMMA. Therefore, the etching rate of photoresist polymers will be faster by using the He/O_2 APPJ. To enlarge the patterning area, it is required to prevent the nanopipette from getting damaged during etching as well as to employ a scanner with a larger scanning area. The nanopipette sometimes got damaged at ignition of the APPJ. The waveform optimization of the applied voltage at ignition of the APPJ will be required in future work.

V. CONCLUSION

In this study, we developed the fine processing method in the submicrometer range using the APPJ with He and additive reactive gas assisted by a scanning probe microscope. The added reactive gas was a small amount of O_2 gas mixed with the plasma He source gas. The etching rate with the additional O_2 gas was several times faster than that without. Optical emission spectroscopy was conducted to investigate the effectiveness of the oxygen radical. At an applied voltage of 3.75 kV and with 0.4 SLM plasma He source gas, the emission intensity of the O atom with an O_2/He ratio of 0.25% O_2 gas was higher than that without O_2. When the flow rate of O_2 gas increased from 1 SCCM to 7 SCCM at an applied voltage of 3.5 kV, the etching rate increased. However, when the flow rate of O_2 gas increased beyond 7 SCCM, the etching rate began to decrease. To maximize the etching rate, it is necessary to optimize the flow rate ratio of O_2 gas to the He source gas. Finally, fine line etching was performed. This process successfully demonstrated submicrometer-width groove etching of the material under atmospheric pressure. The APPJ fine etching method proposed in this study is expected to contribute to the realization of a microfabrication system that is less expensive than the one using focused ion or electron beams.

easily discharged. The introduction of O_2 gas, which is relatively difficult to discharge, causes the energy of the He APPJ to be absorbed by O_2. N_2 gas in air also absorbed the energy of the He APPJ, and the intensity of nitrogen decreased by introducing O_2 gas in Fig. 3. However, the contribution of the nitrogen plasma alone to etching is not significant due to the low reactivity of nitrogen. Thus, the APPJ may become unstable. In a previous study, the instability of the APPJ has been reported.[13] Second, the density of the O atom decreases when the flow rate of O_2 increases. Park et al. reported the simulation of the He/O_2 atmospheric pressure plasma.[26] The density of the generated O atom increases until the flow rate of O_2 gas increases to 0.5%. However, the density decreases as the flow rate increases beyond 0.5%, and the density of O_3 increases. In addition, the critical flow rate increases as the input energy required to generate the

DATA AVAILABILITY

The data that support the findings of this study are available from the corresponding author upon reasonable request.

REFERENCES

[1] S. A. Norberg, E. Johnsen, and M. J. Kushner, J. Appl. Phys. **118**, 013301 (2015).

[2] A. H. Basher and A.-A. H. Mohamed, J. Appl. Phys. **123**, 193302 (2018).

[3] M. Noeske, J. Degenhardt, S. Strudthoff, and U. Lommatzsch, Int. J. Adhes. Adhes. **24**, 171 (2004).

[4] R. Ichiki, T. Inoue, Y. Yoshimitsu, H. Yamamoto, S. Kanda, M. Yoshida, S. Akamine, and S. Kanazawa, IEEE Trans. Plasma Sci. **42**, 2466 (2014).

[5] M. Laroussi and X. Lu, Appl. Phys. Lett. **87**, 113902 (2005).

[6] J. F. Kolb, A.-A. H. Mohamed, R. O. Price, R. J. Swanson, A. Bowman, R. L. Chiavarini, M. Stacey, and K. H. Schoenbach, Appl. Phys. Lett. **92**, 241501 (2008).

[7] S. Kumagai, C.-Y. Chang, J. Jeong, M. Kobayashi, T. Shimizu, and M. Sasaki, Jpn. J. Appl. Phys., Part 1 **55**, 01AF01 (2016).

[8] J. Y. Kim, Y. Wei, J. Li, and S. Kim, Biosens. Bioelectron. **26**, 555 (2010).

[9] M. Teschke, J. Kedzierski, E. G. Finantu-Dinu, D. Korzec, and J. Engemann, IEEE Trans. Plasma Sci. **33**, 310 (2005).

[10] L. Wen, H. Wang, L. He, Q. Zhang, W. Xiang, and J. Chu, Sens. Actuators, A **169**, 362 (2011).

[11] J. Benedikt, K. Focke, A. Yanguas-Gil, and A. von Keudell, Appl. Phys. Lett. **89**, 251504 (2006).

[12] M. Janietz and T. Arnold, Surf. Coat. Technol. **205**, S351 (2011).

[13] T. Saito, R. Mitsuya, Y. Ito, T. Higuchi, and T. Aita, Thin Solid Films **669**, 321 (2019).

[14] H. Paetzelt, G. Böhm, and T. Arnold, Plasma Sources Sci. Technol. **24**, 025002 (2015).

[15] Q. Li, J. Liu, Y. Dai, W. Xiang, M. Zhang, H. Wang, and L. Wen, Micromachines **7**, 232 (2016).

[16] H. Senba, H. Suzuki, and H. Toyoda, Jpn. J. Appl. Phys., Part 1 **58**, SAAC05 (2019).

[17] T. Ichiki, R. Taura, and Y. Horiike, J. Appl. Phys. **95**, 35 (2004).

[18] R. Kakei, A. Ogino, F. Iwata, and M. Nagatsu, Thin Solid Films **518**, 3457 (2010).

[19] T. Abuzairi, M. Okada, S. Bhattacharjee, and M. Nagatsu, Appl. Surf. Sci. **390**, 489 (2016).

[20] T. Wang, J. Liu, B. Yang, X. Chen, X. Wang, and C. Yang, J. Micromech. Microeng. **26**, 065001 (2016).

[21] D. Morimatsu, H. Sugimoto, A. Nakamura, A. Ogino, M. Nagatsu, and F. Iwata, Jpn. J. Appl. Phys., Part 1 **55**, 08NB15 (2016).

[22] J. Y. Kim, H.-B. Gu, Y.-S. Ko, and S.-O. Kim, IEEE Trans. Plasma Sci. **39**, 2302 (2011).

[23] A. Sarani, A. Y. Nikiforov, and C. Leys, Phys. Plasmas **17**, 063504 (2010).

[24] Y.-C. Sung, T.-C. Wei, Y.-C. Liu, and C. Huang, J. Appl. Phys. **57**, 06JH02 (2018).

[25] See https://physics.nist.gov/PhysRefData/ASD/lines_form.html for NIST Atomic Spectra Database.

[26] G. Y. Park, Y. J. Hong, H. W. Lee, J. Y. Sim, and J. K. Lee, Plasma Processes Polym. **7**, 281 (2010).

[27] D. Ellerweg, J. Benedikt, A. von Keudell, N. Knake, and V. Schulz-von der Gathen, New J. Phys. **12**, 013021 (2010).